Mechanical processing and thermal stability of the equiatomic high entropy alloy TiVZrNbHf under vacuum and hydrogen pressure

Lukas Schweiger[a*], Felix Römer[a], Gökhan Gizer[b], Michael Burtscher[a], Daniel Kiener[a],

Claudio Pistidda[b], Alexander Schökel[c], **Florian Spieckermann**[a*], Jürgen Eckert[a,d]

[a] Department of Materials Science, Montanuniversität Leoben, Jahnstraße 12, 8700 Leoben, Austria

[b] Department of Materials Design, Institute of Hydrogen Technology, Helmholtz-Zentrum Hereon GmbH, 21502 Geesthacht, Germany

[c] Deutsches Elektronen-Synchrotron DESY, Notkestr. 85, 22607 Hamburg, Germany

[d] Erich Schmid Institute of Materials Science, Austrian Academy of Sciences, Jahnstraße 12, 8700 Leoben, Austria

*** Corresponding authors: lukas.schweiger@unileoben.ac.at, florian.spieckermann@unileoben.ac.at**

Abstract

This study investigates the potential of nanostructuring the equiatomic high entropy alloy TiVZrNbHf by high-pressure torsion to improve its already promising hydrogen absorption properties. The detailed microstructural analysis of the material after processing demonstrates that a homogenous single-phase nanocrystalline structure was obtained despite shear band development. Due to the metastable character of many high entropy alloys, this analysis was complemented by investigating the thermal stability of the alloy under both vacuum and hydrogen pressure. For the latter, the material was characterized via *in-situ* X-ray diffraction during hydrogen charging at 500 °C, giving a detailed insight into the phase evolution during initial absorption and subsequent cycling. These experiments evidenced the inherent metastability of TiVZrNbHf, which resulted in its decomposition into a bcc, hcp, and C14 Laves phase under both vacuum and hydrogen atmospheres. Despite decomposition, the material retains its nanocrystalline structure under hydrogen pressure, presumably due to hydride formation, while significant grain growth occurs under vacuum. These findings deepen the understanding of the deformation and hydrogen charging behavior of this promising high entropy alloy, suggesting an approach for engineering such alloys for enhanced stability and performance, particularly in solid-state hydrogen storage applications.

Main text

High entropy alloys (HEAs) contain five or more elements in equal or close-to-equal proportions as proposed independently by Cantor and Yeh in 2004.[1,2] Classical metallurgy predicted that such alloys would decompose, forming complex microstructures with intermetallic compounds. However, it was assumed that the high configurational entropy of an HEA can stabilize a single-phase solid solution.[3,4] This was initially confirmed for several HEAs, examples being the Cantor alloy FeCrMnNiCo and the Senkov alloy TiZrHfNbTa.[1,5] Yet, many HEAs are metastable, decomposing at elevated temperatures.[6–8] Nevertheless, HEAs exhibit promising mechanical and functional properties, such as strength-ductility synergy[9–12], high cryogenic toughness[3], hydrogen embrittlement resistance[13], as well as attractive superconductive[14], magnetic[15], and hydrogen storage properties[16,17].

The climate crisis has renewed interest in hydrogen as a green energy carrier, with hydrogen storage becoming a key technology.[18–20] An approach superior to conventional gas and liquid hydrogen storage is solid-state hydrogen storage in metal hydrides.[21,22] High entropy alloys are promising candidate materials potentially offering high storage capacity, easy activation, and tunability of the sorption thermodynamics.[23–25] The absorption properties of many metal hydrides can be improved by mechanical processing, e.g., by high-pressure torsion (HPT)**.** HPT is a convenient pathway for the mechanical synthesis of new HEAs[26] and facilitates the initial hydrogen absorption.[27,28] However, other studies also report trapping of the respective hydride phase.[29]

Plastic deformation introduces lattice defects and induces grain refinement, potentially beneficial for hydrogen absorption. One of the first HEAs investigated in detail is equiatomic TiVZrNbHf.[16,30–33] It can absorb high amounts of hydrogen (2.7 wt.% at 53 bar) but desorbs it completely only above 500 °C.[30] Although thermal instability was reported for TiVZrNbHf for temperatures > 600 °C,[33,34] the temperature region for stable cycling, i.e., 500 °C,[30] was to date not investigated in long-term annealing experiments. Contrary to TiVZrNbHf, newly developed HEAs, including TiZrCrMnFeNi,[29] $Ti_xZr_{2-x}CrMnFeNi$,[35] and $TiV_2ZrCrMnFeNi$,[36] allow for long-term hydrogen absorption and desorption at room temperature (RT) without activation, yet at a significantly lower capacity of about 1.7 wt.%. Nevertheless, exploring high-capacity alloys such as TiVZrNbHf is critical for further developments in

the field. Furthermore, this alloy is a promising candidate for applications requiring high-temperature metal hydrides, such as solar thermal energy storage.[37]

Here, we investigate the application of HPT to bulk equimolar TiVZrNbHf. The resulting nanocrystalline state is highly isotropic, and the small grain size provides excellent statistics in synchrotron X-ray diffraction (XRD) investigations. The as-HPT deformed samples were annealed at 500 °C, both under vacuum and hydrogen atmosphere, and the structural evolution was probed by *in-situ* synchrotron XRD. The results show that the hydrogen has a marked influence on the identified metastable character of the alloy, delaying grain growth but not stopping decomposition from a single-phase to a multi-phase microstructure.

Equiatomic TiVZrNbHf was prepared by melting stoichiometric amounts of granular Ti (99.995 %, HMW Hauner GmbH), V (99.9 %), Zr (99.2 %), Nb (99.9 %), and Hf (99.9 %) in an arc melter (Arc Melter AM 0.5, Edmund Bühler GmbH). Samples were remelted five times for better homogeneity. Disks with a thickness of 1 mm and a diameter of 8 mm were cut from the ingots. HPT was performed on a custom-built device at 7.5 GPa and room temperature (RT) at 1.25 rpm.[38] The HPT anvils had a 0.15 mm deep cavity with a diameter of 8 mm. The torque during HPT was measured for a selected specimen[39] and used for the calculation of the shear stress (see supplementary material).

The sample disks were cut into halves, and the cross-sections were mirror-polished for microstructural characterization. The microstructure was examined by scanning electron microscopy (SEM; LEO type 1525, Carl Zeiss GmbH) and energy dispersive X-ray spectroscopy (EDX; XFlash 6-60, Bruker corporation). On the same cross-sections, the Vickers microhardness $HV_{0.3}$ was determined by employing a universal laboratory hardness tester (DuraScan, ZwickRoell GmbH). Transmission electron microscopy (TEM; JEM-2200FS microscope, JEOL Ltd.) was performed at an axial view in scanning TEM (STEM) mode. Specimens were prepared by polishing and focused-ion beam thinning at radius 3 mm to achieve electron transparency. The annealing experiments under vacuum were done in a vacuum furnace (Xerion Advanced Heating Ofentechnik GmbH, vacuum tube furnace, type Xtube) with $\approx 10^{-6}$ mbar vacuum. The temperature was 500 °C with a heating rate of 10 °C/min and ambient cooling.

XRD was conducted on the P02.1 Powder Diffraction and Total Scattering Beamline of PETRA III (DESY Hamburg). The experiments were done in transmission using a photon energy of 60 keV and a Dectris EIGER2X CdTe 1M-W detector. The calibration was performed with a CeO_2 reference using the pyFAI software.[40] A custom-designed high-pressure cell[41] was used for the *in-situ* loading experiments at elevated temperatures and pressures of up to 50 bar of hydrogen. The heating rate was set to 10 °C/min, and the hydrogen sorption experiments were conducted at 500 °C. Before the experiments, the samples were degassed under vacuum. Peak analysis was performed using the modified Williamson-Hall method (see supplementary material).[42]

Backscatter electron (BSE) micrographs of the as-HPT state are depicted in Figure 1. A lamellar structure is orientated parallel to the shear direction and is related to small chemical heterogeneities likely caused by micro-segregation during the solidification of the HEA.[43,44] Considering the high melting points of refractory HEAs, such as TiVZrNbHf, these chemical heterogeneities are challenging to remove by annealing.[3,45,46] EDX showed that chemical variations were small, within ±2 at.% of the nominal composition (see supplementary material).

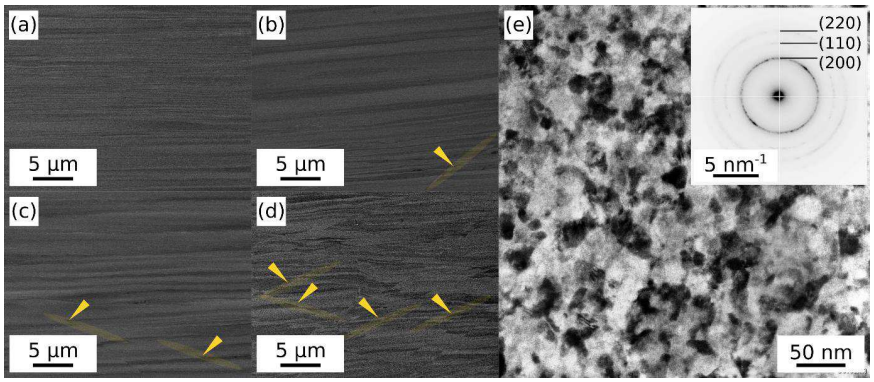

Figure 1: BSE SEM micrographs (cross-section) at a radial position of 3 mm of samples subjected to HPT deformation at RT for (a) 1 (γ≈115), (b) 3 (γ≈346), (c) 10 (γ≈1154) and (d) 30 (γ≈3461) revolutions. Shear bands are highlighted and indicated by arrows. (e) STEM micrograph of the n=30 specimen at a radial position of 3 mm, and the corresponding selected area diffraction pattern as inset.

The microstructure after HPT contains several shear bands, indicated by arrows in Figure 1(b-d). Despite their presence, the deformation does not seem to suffer from persisting deformation localization in a single shear band, and the refinement still results in a homogenous nanostructure. A slight grain contrast was detected at the highest magnifications, indicating a nanocrystalline structure after HPT, as further confirmed by STEM and XRD. The corresponding STEM micrograph after 30 revolutions (*n*) is given in Figure 1 (e) and confirms the nanocrystalline nature of the HEA with a grain size of about 20 nm. Additionally, EBSD patterns (see supplementary material) show a coarse-grained microstrucutre at the disc center, while no grains could be resolved at higher radii and strains.

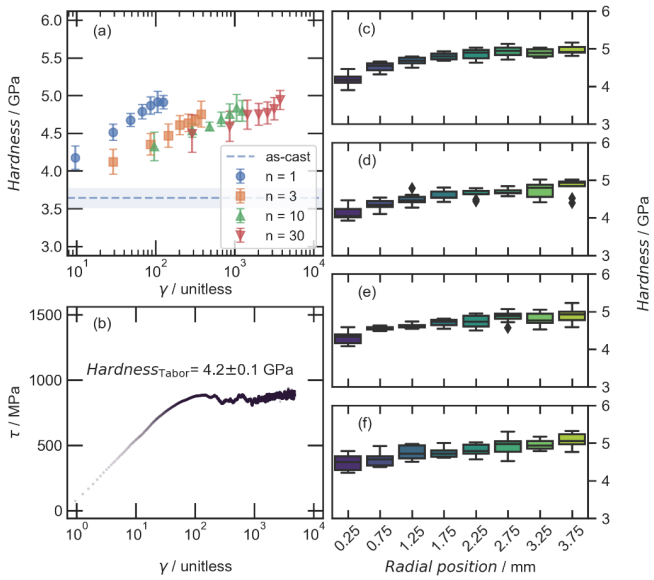

Figure 2: (a) Vickers microhardness as a function of shear strain and (b) the shear stress curve determined from torque measurements during HPT. Box plots of the hardness at certain radii on the HPT disk after (c) 1, (d) 3, (e) 10, and (f) 30 revolutions.

The HPT process can be followed by measuring the microhardness along the radial position after deformation and the torque during deformation, respectively. Figure 2(a) shows the evolution of the HEA microhardness with increasing strain. Initially, the hardness rises strongly, while it remains

unchanged within the error margins above $\gamma \approx 100$, indicating saturation of the microstructure. Nevertheless, a discrepancy between n=1 and after more revolutions is visible, likely due to shear band formation, as shown in Figure 1. Shear bands forming above a certain strain threshold hinder further refinement. This is most evident at lower radii for samples with more revolutions, where no further refinement or hardness saturation occurs despite higher nominal strains.

The torque measurement allows the calculation of flow curves, as conducted in Figure 2(b). Initially, the shear stress increases rapidly due to strain hardening, followed by a steady-state stress level. No strain softening or slip-stick events were observed, and the material exhibits a distinct shear stress plateau. Figure 2(c-f) gives a detailed overview of the hardness evolution over the radial position within the HPT disks. For 1 and 3 revolutions, only a minor hardness gradient as a function of radius is evident, reducing and vanishing for radii > 1 mm (Figure 2(f)) after 30 revolutions. Consequently, HPT deforms the HEA TiVZrNbHf in a controlled manner, and a uniform nanocrystalline microstructure is achieved throughout most of the HPT disk at strains exceeding 100.

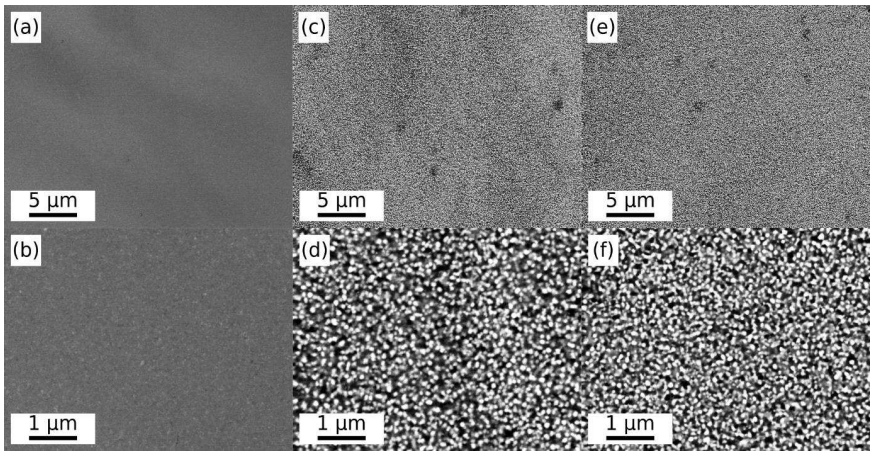

Figure 3: BSE SEM micrographs (top-view) at a radial position of 3 mm of samples after vacuum annealing for (a, b) 1 h, (c, d) 10 h, and (e, f) 30 h at 500 °C.

After HPT, the samples were vacuum annealed for 1 h, 10 h, and 30 h. The corresponding micrographs are shown in Figure 3. After annealing at 500 °C for 10 h, the microstructure consists of significantly

larger grains in the ultra-fine grained regime (100-1000 nm)[47] with grain sizes of 100-120 nm. Distinct bright and dark regions indicate a decomposition into two or more phases. Interestingly, the grain size changes only marginally from 10 h to 30 h annealing time. The complex-phase microstructure, therefore, exhibits significant thermal stability against grain growth after the initial decomposition.

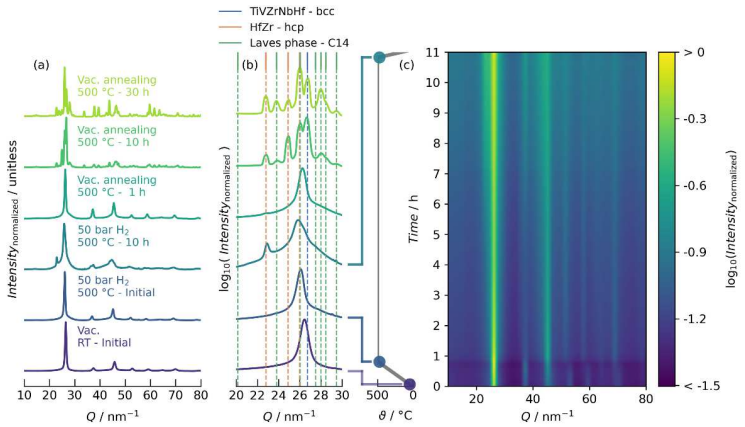

Figure 4: (a) Synchrotron XRD patterns of TiVZrNbHf before and after annealing at 500 °C under vacuum or 50 bar hydrogen with (b) a magnified region of interest plotted on a logarithmic scale. (c) *In-situ* XRD measurements of the hydrogen absorption at 500 °C and 50 bar hydrogen with logarithmic color scaling.

Synchrotron XRD measurements were conducted on samples after vacuum annealing at 500 °C, and *in-situ* annealing experiments were performed under 50 bar hydrogen, thereby probing the competition between hydrogen absorption and microstructural decomposition. Figure 4(a) compares the XRD patterns before/after annealing under vacuum and before/after annealing for 10 h under 50 bar of hydrogen, respectively. As previously reported, the HEA in the as-HPT state consists of a single bcc phase. The modified Williamson-Hall analysis yields a crystallite size of 51 nm ± 39 nm and microstrains of 5.8 % ± 0.44 %, equivalent to a dislocation density of $2.6 \cdot 10^{16}$ m^{-2} ± $4.0 \cdot 10^{15}$ m^{-2}. Despite the significant standard deviation of the domain size, it can be stated that the as-HPT state is nanocrystalline and dislocation-rich.

There is a clear difference between the samples annealed under vacuum and hydrogen atmosphere. Figure 4(a,b) shows that the vacuum-annealed samples exhibit pronounced decomposition and contain

a bcc, hcp, and C14 Laves phase, in agreement with a previous study.[33] Additionally, the patterns show narrow, well-defined peaks, indicating grain growth/recrystallization, in line with the micrographs in Figure 3.

In a previous study,[30] *in-situ* XRD measurements during hydrogen cycling at 500 °C were performed, showing stable cycling, i.e., absorption and desorption, within a timeframe of less than 2 h. Thereby, the material was ball-milled, and it absorbed hydrogen rapidly at 250 °C.[30] Other studies reported that the first absorption can be conducted within 48 h at 400 °C and 20 bar hydrogen.[16] To stay comparable with the vacuum annealing experiments, we subjected the as-HPT bulk material to hydrogen at cycling conditions, i.e., 500 °C. After 10 h, absorption was still incomplete, likely due to the insufficient diffusivity of the hydrogen or a lack of activation. A distinct peak appeared at 23 nm^{-1}, visible in Figure 4(b,c). Due to the broad and overlapping peaks, it was challenging to unambiguously associate this single peak with any particular phase. One reason could be the formation of a hydride with a comparably high driving force or low kinetic barrier for nucleation. The peak coincides with the first peak of many elemental hydrides, e.g., TiH_2, but also hydrides such as D_xV_2Zr. However, more likely, the peak could be related to the formation of the hcp phase discussed above. The HEA did not exhibit significant grain growth under hydrogen atmosphere, as no peak narrowing was observed under such conditions. On the contrary, overall, the peaks broaden, possibly masking other minor peaks associated with decomposition.

For the vacuum-annealed samples, three distinct peaks in the low Q region (see supplementary material) are associated with the C14 Laves phase, while under hydrogen, only a broad hump is observable. This highlights that phase decomposition occurs but also that grain growth/recrystallization is impeded. Therefore, we conclude that many of the peaks associated with the phase decomposition are contained within the convolution of broad peaks, with a clear deconvolution being, unfortunately, not possible.

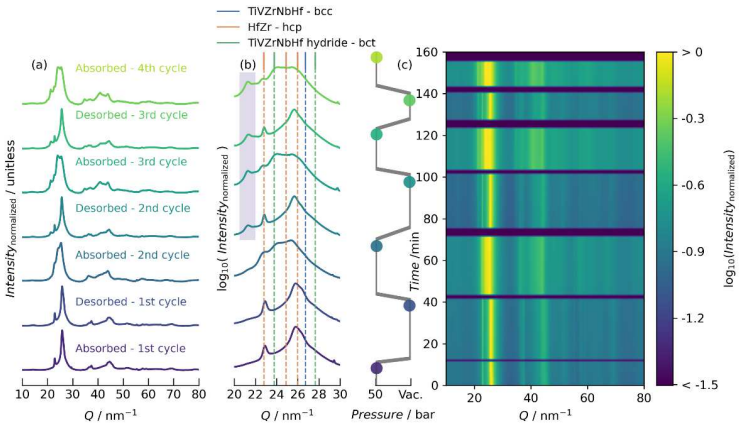

Figure 5: (a) Synchrotron XRD patterns of TiVZrNbHf during cycling between vacuum and 50 bar hydrogen with (b) a magnified region of interest plotted on a logarithmic scale. (c) *In-situ* XRD measurements of the hydrogen cycling at 500 °C with logarithmic color scaling.

After 10 hours at 500 °C and 50 bar of hydrogen, the sample was cooled down to RT under pressure. Subsequently, pressure-cycling between vacuum (desorption) and 50 bar hydrogen (absorption) at a constant temperature of 500 °C was performed, as plotted in Figure 5. The initial absorption was sluggish and incomplete, leading to a first desorption with insignificant changes. However, the second absorption (1st cycle) resulted in the rapid formation of a hydride phase on, albeit only partial, hydrogenation, see Figure 5(b). As the material pulverized during the *in-situ* experiment, we associate this absorption tipping point with fracture of the bulk sample, generating faster diffusion pathways. Consecutive cycling exhibits stable and reproducible formation of the hydride phase, confirming the cyclability of HPT deformed TiVZrNbHf. However, an additional phase forms after the first cycle, with peaks in the range of 21, 35, and 41 nm^{-1}, relatively stable in subsequent cycles, see Figure 5(b). This might be associated with another, more stable hydride that does not desorb at 500 °C and vacuum, possibly derived from one of the decomposition products.

The structural investigation after HPT proves the refinement of the HEA TiVZrNbHf into a homogeneous nanocrystalline state. The SEM images reveal shear bands, visible in Figure 1(b,c,d), proving that the alloy does not exhibit fully homogeneous plasticity[48] as could be expected from the

flow curve in Figure 2(b). Rather, the plateau might be associated with the continuous formation of shear bands, as many are visible in Figure 1(c,d). Nevertheless, except for regions close to the disk center, the HEA already arrives at a nanocrystalline state before shear band generation might hinder the refinement. This limited refinement at lower radii can explain the discrepancy between the samples deformed for 1 and 3 revolutions.

The results highlight that the HEA TiVZrNbHf can be easily mechanically processed, which may improve its hydrogen sorption properties. Further investigations of the detailed hydrogen sorption properties of TiVZrNbHf after HPT are underway. However, the sluggish absorption shown in Figure 4(c) indicates that HPT does not improve the initial absorption kinetics, despite being reported for other HEA systems.[27] Studies on TiVZrNbHf and similar bcc HEAs characterized crushed[49,50] or ball milled[16,30] powders handled under Ar atmosphere and report fast initial absorption after activation at elevated temperatures[31,49] or by off-stochiometric compositions[50]. Unfortunately, HPT does not seem to impact the activation behavior. Nevertheless, the current results highlight the importance of the alloy composition and, in particular, the surface state, more specifically the oxide layer, for initial absorption. The annealing experiments of the as-HPT sample at 500 °C under vacuum reveal the inherent metastability of TiVZrNbHf as the single-phase bcc material decomposes into bcc, hcp, and C14 Laves phases, see Figure 4(a). While previous studies highlighted rapid decomposition at temperatures exceeding 600 °C,[33] they did not consider long-term annealing at 500 °C. Nevertheless, these phases are in line with those reported by Pacheco *et al.* for the decomposition of the same material but at temperatures > 600 °C.[33] The authors reported ZrHf for the hcp, V_2(Hf,Zr,Nb) for the C14, and a V-lean bcc solid solution phase. Similar instabilities were also reported for other bcc HEAs, notably the similar alloy TiVZrNbTa, decomposing at 800 °C after cold rolling or HPT.[7,51] Both studies identified the formation of Zr-Hf (bcc and hcp) and a Nb-Ta-rich phase. Indeed, in this study, the chemical composition of the hcp phase is ZrHf; the Laves phase was fitted without any chemical information. A notable difference is that the lattice constant of the remaining bcc phase was reported to increase with decomposition,[33] while we observed a respective decrease in our study. Consequently, the decomposition phases differ significantly in chemical composition, which is the origin of the contrast

differences in Figure 3. As the temperature allowing for complete hydrogen desorption of this HEA is 500 °C,[16,30] this highlights that the HEA is thermodynamically unstable under non-hydrogen conditions at cycling temperatures, potentially deteriorating the hydrogen sorption properties and impairing its application.

In contrast, at a pressure of 50 bar hydrogen, the evolution of the microstructure changed significantly. Figure 4 depicts that the XRD pattern changes after 10 h at 500 °C at 50 bar hydrogen, but not as drastically compared to annealing under vacuum. The peak broadening can be associated with the strains that are introduced by hydrogen absorption into the metallic lattice but also by the possible decomposition of the bcc phase and formation of a complex nanoscale and multi-phase structure, respectively. Both effects will overlap, forming a highly convoluted pattern, as seen in Figures 4 and 5. Nevertheless, the results indicate a limitation of recrystallization/grain growth, resulting in a stabilization of the nanocrystalline structure.

In line with the *defectant model*,[52,53] we suggest that hydrogen diffuses into the HEA to defect sites, i.e., dislocations, vacancies, and grain boundaries.[54] These interactions are responsible for many hydrogen-related effects, most notably hydrogen embrittlement.[55,56] Pinning vacancies and grain boundaries should limit the potential of phase transformations and grain growth, as reported for HPT deformed Pd.[57] However, Martin *et al*. report the opposite for vanadium, i.e., hydrogen-induced accelerated grain growth.[58] They argued that hydrogen reduces the thermodynamic driving force for grain growth but increases grain boundary mobility by facilitating the formation of ledges during grain boundary migration while concomitantly stabilizing vacancies necessary for accommodating the free volume generated during grain growth.[58] That study was performed under conditions not favoring hydride formation.[59] In the present case, an additional effect could be the formation of hydride precipitates close to grain boundaries, providing additional pinning features. As discussed above, the unidentified peaks might be associated with such (elemental) hydrides, which might originate from chemical heterogeneities at the nanoscale. Ti-Zr and Nb-Hf clusters were reported for similar HEAs, namely TiZrHfNb.[60] This short-range ordering was linked to the occurrence of (Ti,Zr,O)-enriched complexes and could lead to the formation of similar (Ti,Zr,H)-hydrides.[60] We conclude that the formation of

hydrides must be the reason for the retained grain growth. Thus, despite the metastable character of the TiVZrNbHf alloy, it might still be possible to stabilize the microstructure by the hydride formation itself.

In general, the present results broaden the understanding of hydrogen storage in HEAs and the respective interactions in nanocrystalline HEAs and open another viable route for engineering HEAs and other materials for the highest stability and performance.

In conclusion, the investigated TiVZrNbHf HEA subjected to HPT reveals the formation of a homogeneous nanocrystalline state despite the formation of multiple shear bands at higher strains. Therefore, the alloy exhibits potential for mechanical processing, possibly promoting defect-facilitated hydrogen sorption properties. However, annealing experiments indicate inherent metastability under non-hydrogen conditions, leading to phase decomposition. Interestingly, under 50 bar hydrogen pressure, the alloy shows a stabilized structure under cyclic charging conditions, indicating the role of hydrogen in impeding grain growth via pinning by hydrides. This finding opens avenues for using hydrogen as a stabilizing factor in HEAs, enabling new possibilities for solid-state hydrogen storage and structural materials with enhanced stability and performance.

Supplementary material

See the supplementary material for detailed methods and additional experimental results (EDX, EBSD, XRD).

Acknowledgments

This research activity is part of the Strategic Core Research Area SCoRe A+ Hydrogen and Carbon and has received funding from Montanuniversität Leoben. We acknowledge DESY (Hamburg, Germany), a member of the Helmholtz Association HGF, for the provision of experimental facilities. Parts of this research were carried out at PETRA III using beamline P02.1. Beamtime was allocated for proposal I-20230216 EC. We gratefully acknowledge the support of Eray Yüce and Yuanyuan Shang.

Conflict of Interest Statement

The authors have no conflicts to disclose.

Author Contributions

Lukas Schweiger: Conceptualization (equal); Investigation (equal); Data Curation (equal); Formal analysis (equal); Visualization (equal); Writing - Original Draft (lead). **Felix Römer:** Investigation (equal); Data Curation (equal); Writing - Review & Editing (supporting). **Gökhan Gizer:** Investigation (equal); Resources (equal); Writing - Review & Editing (supporting). **Michael Burtscher:** Investigation (supporting); Formal analysis (supporting); Writing - Review & Editing (supporting). **Daniel Kiener:** Conceptualization (equal); Supervision (equal); Validation (equal); Writing - Review & Editing (equal). **Claudio Pistidda:** Resources (equal); Writing - Review & Editing (supporting). **Alexander Schökel:** Resources (equal); Writing - Review & Editing (supporting). **Florian Spieckermann:** Conceptualization (lead); Supervision (equal); Validation (equal); Resources (equal); Writing - Review & Editing (equal). **Jürgen Eckert:** Conceptualization (equal); Supervision (equal); Writing - Review & Editing (equal)

DATA AVAILABILITY

The data that support the findings of this study are available from the corresponding author upon reasonable request.

References

[1] B. Cantor, I.T.H. Chang, P. Knight, and A.J.B. Vincent, "Microstructural development in equiatomic multicomponent alloys," Mater. Sci. Eng. A **375–377**(1-2 SPEC. ISS.), 213–218 (2004).

[2] J.W. Yeh, S.K. Chen, S.J. Lin, J.Y. Gan, T.S. Chin, T.T. Shun, C.H. Tsau, and S.Y. Chang, "Nanostructured high-entropy alloys with multiple principal elements: Novel alloy design concepts and outcomes," Adv. Eng. Mater. **6**(5), 299–303 (2004).

[3] E.P. George, D. Raabe, and R.O. Ritchie, "High-entropy alloys," Nat. Rev. Mater. **4**(8), 515–534 (2019).

[4] F. Otto, Y. Yang, H. Bei, and E.P. George, "Relative effects of enthalpy and entropy on the phase stability of equiatomic high-entropy alloys," Acta Mater. **61**(7), 2628–2638 (2013).

[5] O.N. Senkov, J.M. Scott, S. V. Senkova, D.B. Miracle, and C.F. Woodward, "Microstructure and room temperature properties of a high-entropy TaNbHfZrTi alloy," J. Alloys Compd. **509**(20), 6043–6048 (2011).

[6] B. Schuh, F. Mendez-Martin, B. Völker, E.P. George, H. Clemens, R. Pippan, and A. Hohenwarter, "Mechanical properties, microstructure and thermal stability of a nanocrystalline CoCrFeMnNi high-entropy alloy after severe plastic deformation," Acta Mater. **96**, 258–268 (2015).

[7] B. Schuh, B. Völker, J. Todt, N. Schell, L. Perrière, J. Li, J.P. Couzinié, and A. Hohenwarter, "Thermodynamic instability of a nanocrystalline, single-phase TiZrNbHfTa alloy and its impact on the mechanical properties," Acta Mater. **142**, 201–212 (2018).

[8] F. Otto, A. Dlouhý, K.G. Pradeep, M. Kuběnová, D. Raabe, G. Eggeler, and E.P. George, "Decomposition of the single-phase high-entropy alloy CrMnFeCoNi after prolonged anneals at intermediate temperatures," Acta Mater. **112**, 40–52 (2016).

[9] Z. Li, K.G. Pradeep, Y. Deng, D. Raabe, and C.C. Tasan, "Metastable high-entropy dual-phase alloys overcome the strength-ductility trade-off," Nature **534**(7606), 227–230 (2016).

[10] E.P. George, W.A. Curtin, and C.C. Tasan, "High entropy alloys: A focused review of mechanical properties and deformation mechanisms," Acta Mater. **188**, 435–474 (2020).

[11] N. Chawake, L. Raman, P. Ramasamy, P. Ghosh, F. Spieckermann, C. Gammer, B.S. Murty, R.S. Kottada, and J. Eckert, "Composite of medium entropy alloys synthesized using spark plasma sintering," Scr. Mater. **191**, 46–51 (2021).

[12] Y. Shang, J. Brechtl, C. Pistidda, and P.K. Liaw, in *High-Entropy Mater. Theory, Exp. Appl.* (Springer International Publishing, Cham, 2021), pp. 435–522.

[13] H. Luo, Z. Li, and D. Raabe, "Hydrogen enhances strength and ductility of an equiatomic high-entropy alloy," Sci. Rep. **7**(1), 1–7 (2017).

[14] L. Sun, and R.J. Cava, "High-entropy alloy superconductors: Status, opportunities, and challenges," Phys. Rev. Mater. **3**(9), 090301 (2019).

[15] L. Han, F. Maccari, I.R. Souza Filho, N.J. Peter, Y. Wei, B. Gault, O. Gutfleisch, Z. Li, and D. Raabe, "A mechanically strong and ductile soft magnet with extremely low coercivity," Nature **608**(7922), 310–316 (2022).

[16] M. Sahlberg, D. Karlsson, C. Zlotea, and U. Jansson, "Superior hydrogen storage in high entropy alloys," Sci. Rep. **6**, 1–6 (2016).

[17] Y. Shang, Z. Lei, E. Alvares, S. Garroni, T. Chen, R. Dore, M. Rustici, S. Enzo, A. Schökel, Y. Shi, P. Jerabek, Z. Lu, T. Klassen, and C. Pistidda, "Ultra-lightweight compositionally complex alloys with large ambient-temperature hydrogen storage capacity," Mater. Today **xxx**(xx), (2023).

[18] D. Castelvecchi, "How the hydrogen revolution can help save the planet — and how it can't," Nature **611**(7936), 440–443 (2022).

[19] J. Andersson, and S. Grönkvist, "Large-scale storage of hydrogen," Int. J. Hydrogen Energy **44**(23), 11901–11919 (2019).

[20] Bloomberg NEF, *Hydrogen Economy Outlook - Key Messages* (2020).

[21] N. Klopčič, I. Grimmer, F. Winkler, M. Sartory, and A. Trattner, "A review on metal hydride materials for hydrogen storage," J. Energy Storage **72**(July), (2023).

[22] L. Schlapbach, and A. Züttel, "Hydrogen-storage materials for mobile applications," Nature **414**(6861), 353–358 (2001).

[23] F. Marques, M. Balcerzak, F. Winkelmann, G. Zepon, and M. Felderhoff, "Review and outlook on high-entropy alloys for hydrogen storage," Energy Environ. Sci. **14**(10), 5191–5227 (2021).

[24] B. Sarac, V. Zadorozhnyy, Y.P. Ivanov, F. Spieckermann, S. Klyamkin, E. Berdonosova, M. Serov, S. Kaloshkin, A.L. Greer, A.S. Sarac, and J. Eckert, "Transition metal-based high entropy alloy microfiber electrodes: Corrosion behavior and hydrogen activity," Corros. Sci. **193**(October), 109880 (2021).

[25] M. Witman, G. Ek, S. Ling, J. Chames, S. Agarwal, J. Wong, M.D. Allendorf, M. Sahlberg, and V. Stavila, "Data-Driven Discovery and Synthesis of High Entropy Alloy Hydrides with Targeted Thermodynamic Stability," Chem. Mater., (2021).

[26] K. Edalati, H.W. Li, A. Kilmametov, R. Floriano, and C. Borchers, "High-pressure torsion for synthesis of high-entropy alloys," Metals (Basel). **11**(8), 1–12 (2021).

[27] J. Hidalgo-Jimenez, J.M. Cubero-Sesin, K. Edalati, S. Khajavi, and J. Huot, "Effect of high-pressure torsion on first hydrogenation of Laves phase Ti0.5Zr0.5(Mn1-Fe)Cr1 (x = 0, 0.2 and 0.4) high entropy alloys," J. Alloys Compd. **969**(September), 172243 (2023).

[28] M.O. de Marco, Y. Li, H.W. Li, K. Edalati, and R. Floriano, "Mechanical Synthesis and Hydrogen Storage Characterization of MgVCr and MgVTiCrFe High-Entropy Alloy," Adv. Eng. Mater. **22**(2), (2020).

[29] P. Edalati, R. Floriano, A. Mohammadi, Y. Li, G. Zepon, H.W. Li, and K. Edalati, "Reversible room temperature hydrogen storage in high-entropy alloy TiZrCrMnFeNi," Scr. Mater. **178**, 387–390 (2020).

[30] D. Karlsson, G. Ek, J. Cedervall, C. Zlotea, K.T. Møller, T.C. Hansen, J. Bednarčík, M. Paskevicius, M.H. Sørby, T.R. Jensen, U. Jansson, and M. Sahlberg, "Structure and Hydrogenation Properties of a HfNbTiVZr High-Entropy Alloy," Inorg. Chem. **57**(4), 2103–2110 (2018).

[31] G. Ek, M.M. Nygård, A.F. Pavan, J. Montero, P.F. Henry, M.H. Sørby, M. Witman, V. Stavila, C. Zlotea, B.C. Hauback, and M. Sahlberg, "Elucidating the Effects of the Composition on Hydrogen Sorption in TiVZrNbHf-Based High-Entropy Alloys," Inorg. Chem. **60**(2), 1124–1132 (2021).

[32] M.M. Nygård, W.A. Sławiński, G. Ek, M.H. Sørby, M. Sahlberg, D.A. Keen, and B.C. Hauback, "Local order in high-entropy alloys and associated deuterides – a total scattering and Reverse Monte Carlo study," Acta Mater. **199**, 504–513 (2020).

[33] V. Pacheco, G. Lindwall, D. Karlsson, J. Cedervall, S. Fritze, G. Ek, P. Berastegui, M. Sahlberg, and U. Jansson, "Thermal Stability of the HfNbTiVZr High-Entropy Alloy," Inorg. Chem. **58**(1), 811–820

(2019).

[34] S. Fritze, C.M. Koller, L. von Fieandt, P. Malinovskis, K. Johansson, E. Lewin, P.H. Mayrhofer, and U. Jansson, "Influence of deposition temperature on the phase evolution of HfNbTiVZr high-entropy thin films," Materials (Basel). **12**(4), 10–17 (2019).

[35] A. Mohammadi, Y. Ikeda, P. Edalati, M. Mito, B. Grabowski, H.-W. Li, and K. Edalati, "High-entropy hydrides for fast and reversible hydrogen storage at room temperature: Binding-energy engineering via first-principles calculations and experiments," Acta Mater. **236**, 118117 (2022).

[36] S. Dangwal, and K. Edalati, "High-entropy alloy TiV2ZrCrMnFeNi for hydrogen storage at room temperature with full reversibility and good activation," Scr. Mater. **238**(September 2023), 115774 (2024).

[37] D.A. Sheppard, M. Paskevicius, T.D. Humphries, M. Felderhoff, G. Capurso, J. Bellosta von Colbe, M. Dornheim, T. Klassen, P.A. Ward, J.A. Teprovich, C. Corgnale, R. Zidan, D.M. Grant, and C.E. Buckley, "Metal hydrides for concentrating solar thermal power energy storage," Appl. Phys. A Mater. Sci. Process. **122**(4), 1–15 (2016).

[38] A. Hohenwarter, A. Bachmaier, B. Gludovatz, S. Scheriau, and R. Pippan, "Technical parameters affecting grain refinement by high pressure torsion," Int. J. Mater. Res. **100**(12), 1653–1661 (2009).

[39] H.-P. Stüwe, and H. Turck, "Zur Messung von Fließkurven im Torsionsversuch," Int. J. Mater. Res. **55**(11), 699–703 (1964).

[40] G. Ashiotis, A. Deschildre, Z. Nawaz, J.P. Wright, D. Karkoulis, F.E. Picca, and J. Kieffer, "The fast azimuthal integration Python library: pyFAI," J. Appl. Crystallogr. **48**(2), 510–519 (2015).

[41] U. Bösenberg, C. Pistidda, M. Tolkiehn, N. Busch, I. Saldan, K. Suarez-Alcantara, A. Arendarska, T. Klassen, and M. Dornheim, "Characterization of metal hydrides by in-situ XRD," Int. J. Hydrogen Energy **39**(18), 9899–9903 (2014).

[42] T. Ungár, and A. Borbély, "The effect of dislocation contrast on x-ray line broadening: A new approach to line profile analysis," Appl. Phys. Lett. **69**(21), 3173–3175 (1996).

[43] T. Vlasák, J. Čížek, O. Melikhova, F. Lukáč, D. Preisler, M. Janeček, P. Harcuba, M. Zimina, and O. Srba, "Thermal Stability of Microstructure of High-Entropy Alloys Based on Refractory Metals Hf, Nb, Ta, Ti, V, and Zr," Metals (Basel). **12**(3), (2022).

[44] E. Fazakas, V. Zadorozhnyy, L.K. Varga, A. Inoue, D. V. Louzguine-Luzgin, F. Tian, and L. Vitos, "Experimental and theoretical study of Ti20Zr20Hf 20Nb20X20 (X = v or Cr) refractory high-entropy alloys," Int. J. Refract. Met. Hard Mater. **47**, 131–138 (2014).

[45] O.N. Senkov, G.B. Wilks, D.B. Miracle, C.P. Chuang, and P.K. Liaw, "Refractory high-entropy alloys," Intermetallics **18**(9), 1758–1765 (2010).

[46] O.N. Senkov, G.B. Wilks, J.M. Scott, and D.B. Miracle, "Mechanical properties of Nb25Mo25Ta 25W25 and V20Nb20Mo 20Ta20W20 refractory high entropy alloys," Intermetallics **19**(5), 698–706 (2011).

[47] R.Z. Valiev, Y. Estrin, Z. Horita, T.G. Langdon, M.J. Zehetbauer, and Y. Zhu, "Producing Bulk Ultrafine-Grained Materials by Severe Plastic Deformation," Jom **58**(4), 33–39 (2006).

[48] Y. Beygelzimer, Y. Estrin, and R. Kulagin, "Some Unresolved Problems of High-Pressure Torsion," Mater. Trans. **64**(8), MT-MF2022038 (2023).

[49] S. Sleiman, and J. Huot, "Effect of particle size, pressure and temperature on the activation process of hydrogen absorption in TiVZrHfNb high entropy alloy," J. Alloys Compd. **861**, 158615 (2021).

[50] S. Sleiman, and J. Huot, "Microstructure and First Hydrogenation Properties of TiHfZrNb1-xV1+x Alloy for x = 0, 0.1, 0.2, 0.4, 0.6 and 1," Molecules **27**(3), 1–14 (2022).

[51] O.N. Senkov, and S.L. Semiatin, "Microstructure and properties of a refractory high-entropy alloy after cold working," J. Alloys Compd. **649**, 1110–1123 (2015).

[52] R. Kirchheim, "On the solute-defect interaction in the framework of a defactant concept," Int. J. Mater. Res. **100**(4), 483–487 (2009).

[53] R. Kirchheim, "Solid solution softening and hardening by mobile solute atoms with special focus on hydrogen," Scr. Mater. **67**(9), 767–770 (2012).

[54] A. Pundt, and R. Kirchheim, "Hydrogen in metals: Microstructural aspects," Annu. Rev. Mater. Res. **36**(10), 555–608 (2006).

[55] S. Lynch, "Hydrogen embrittlement phenomena and mechanisms," Corros. Rev. **30**(3–4), 105–123 (2012).

[56] B. Sun, D. Wang, X. Lu, D. Wan, D. Ponge, and X. Zhang, "Current Challenges and Opportunities Toward Understanding Hydrogen Embrittlement Mechanisms in Advanced High-Strength Steels: A Review," Acta Metall. Sin. (English Lett. **34**(6), 741–754 (2021).

[57] M. Krystian, D. Setman, B. Mingler, G. Krexner, and M.J. Zehetbauer, "Formation of superabundant vacancies in nano-Pd-H generated by high-pressure torsion," Scr. Mater. **62**(1), 49–52 (2010).

[58] M.L. Martin, A. Pundt, and R. Kirchheim, "Hydrogen-induced accelerated grain growth in vanadium," Acta Mater. **155**, 262–267 (2018).

[59] S. Kumar, G.P. Tiwari, and N. Krishnamurthy, "Tailoring the hydrogen desorption thermodynamics of V2H by alloying additives," J. Alloys Compd. **645**(S1), S252–S256 (2015).

[60] B. Zhang, J. Ding, and E. Ma, "Chemical short-range order in body-centered-cubic TiZrHfNb high-entropy alloys," Appl. Phys. Lett. **119**(20), (2021).

[61] M.J. Zehetbauer, J. Kohout, E. Schafler, F. Sachslehner, and A. Dubravina, "Plastic deformation of nickel under high hydrostatic pressure," J. Alloys Compd. **378**(1–2), 329–334 (2004).

[62] U.F. Kocks, "The relation between polycrystal deformation and single-crystal deformation," Metall. Trans. **1**(5), 1121–1143 (1970).

[63] T. Ungár, I. Dragomir, Á. Révész, and A. Borbély, "The contrast factors of dislocations in cubic crystals: The dislocation model of strain anisotropy in practice," J. Appl. Crystallogr. **32**(5), 992–1002 (1999).

[64] L.Y. Tian, G. Wang, J.S. Harris, D.L. Irving, J. Zhao, and L. Vitos, "Alloying effect on the elastic properties of refractory high-entropy alloys," Mater. Des. **114**, 243–252 (2017).

[65] A. Borbély, "The modified Williamson-Hall plot and dislocation density evaluation from diffraction peaks," Scr. Mater. **217**(February), 114768 (2022).